Journal of Materials Chemistry C

Accepted Manuscript

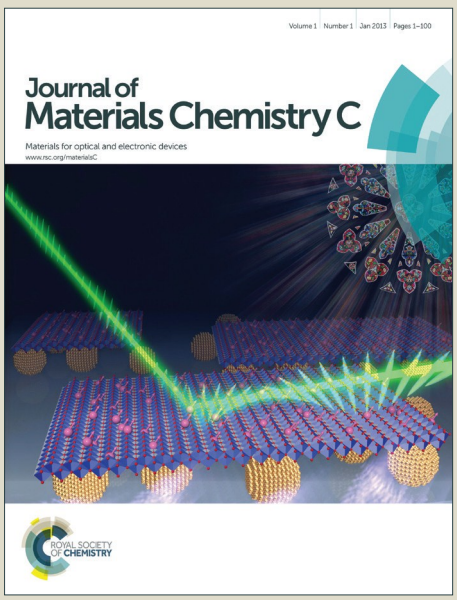

ROYAL SOCIETY OF CHEMISTRY

www.rsc.org/materialsC

Solution synthesis of GeS and GeSe nanosheets for high-sensitivity photodetectors

Parthiban Ramasamy, Dohyun Kwak, Da-Hye Lim, Hyun-Soo Ra, and Jong-Soo lee*

Department of Energy Systems Engineering, DGIST, Daegu, 711-873, Republic of Korea

E-mail: jslee@dgist.ac.kr

Abstract

We report the synthesis of 2D nanosheets of GeS and GeSe by facile solution based approaches. The synthesized nanosheets are single-crystalline in nature with lateral dimensions in micrometers. Band structures calculated from DFT calculations predicted a direct bandgap value of 1.67 and 1.37 eV for GeS and GeSe, respectively. The experimental bandgap values (GeS, E_g=1.6 eV and GeSe, E_g=1.2 eV) determined from optical measurements are slightly smaller than the predicted ones. Photoresponse measurements of GeS and GeSe nanosheets revealed that the nanosheets are extremely photoresponsive for the incident light and exhibit high photoresponsivity up to 173 and 870 AW^{-1} under 405 nm laser diode, respectively. These values are several orders of magnitude higher than that of previous reports for graphene and many other metal chalcogenide nanosheet photodetectors. In addition, the photodetectors have fast photoresponse time and specific detectivity in the order of 10^{13} Jones. These results show that both the GeS and GeSe nanosheets are promising narrow bandgap semiconductors for high performance photodetectors.

1. Introduction

Over the past decade, two-dimensional (2D) nanostructures have been extensively studied as prospective candidates for the application in photovoltaics, field effect transistors, batteries, and photodetectors.[1-5] Graphene, one of the most studied 2D material has exhibited excellent performance in electronic and optoelectronic devices, as well as sensors.[6-8] Despite its array of exciting properties, the lack of bandgap in graphene results in weaker light absorption and fast recombination of photogenerated carries, which limits its application in optoelectronic devices especially photodetectors. Hence, there has been a growing interest in 2D metal chalcogenides with an intrinsic bandgap for the application in optoelectronics.[9-13] In this context, various transition metal chalcogenides (TMC) with layered structured (i.e. MoS_2, $MoSe_2$, GaS, GaSe and In_2Se_3) have been proposed as alternative 2D systems and exhibited better performance in photodetectors.[14-20] For example, ultrasensitive photoresponse has been observed in monolayer MoS_2 with photoresponsivities reaching 880 A/W.[14] In_2Se_3 nanosheets also exhibited high photoresponsivity of 395 A/W and an external quantum efficiency of 1.63×10^5 % at 5 V bias.[19] These findings demonstrate the potential of 2D inorganic chalcogenide nanosheets for applications in high performance electronics and optoelectronics.

Recently, narrow bandgap IV-VI semiconductor nanostructures such as SnS, SnSe, GeS, GeSe have attracted strong interest in optoelectronics.[21,22] The Ge-based chalcogenides (i.e. GeS, GeSe) are potential alternatives for Cd and Pb-based nanostructures due to their relative earth abundant constituents and low toxicity. Both the GeS and GeSe are p-type semiconductors with orthorhombic layered crystal structure, which can be considered as a distorted NaCl structure. They have strong covalent bonding within the layer and weak van der Walls interactions between the adjacent layers, which facilitates the growth of 2D nanostructures in these systems. The bandgaps for GeS and GeSe have been reported to be in

the range of 1.55-1.65 eV and 1.1-1.2 eV, respectively.[23,24] These values match well with the desired absorption range for an efficient photovoltaic material. Besides optoelectronic applications, GeS and GeSe nanostructures have also exhibited excellent Li ion storage properties.[25-27] However, only limited studies have been published on GeS and GeSe nanostructures compared to that of other IV-VI semiconductors such as lead or tin-based chalcogenides. This is due to the difficulties associated with the synthesis of GeS and GeSe nanostructures. Only few reports have been published for the synthesis of these nanostructures and most of them are based on physical methods such as vapor deposition techniques.[28-31] There also few solution based methods available for GeSe nanostructures, however only one article has reported the colloidal synthesis of GeS nanosheets.[32-35] Solution based methods are more suitable for large scale production and the resulting nanostructures can be dispersed in variety of solvents, which can be used to fabricate large area optoelectronic devices by simple solution processing techniques. Given the growing interest in the potential applications of GeS and GeSe nanostructures, it is highly necessary to develop simple and new methods to synthesize these nanostructures to evaluate their applications in optoelectronics.

Herein, we report solution based synthetic strategies for micrometer sized GeS and GeSe nanosheets. The as-synthesized nanosheets were used to fabricate photodetectors on Si/SiO_2 substrate. Both the GeS and GeSe photodetectors show highly photosensitive, fast and stable photoresponse under 405 nm laser diode. Highest responsivity of 870 AW^{-1} with an EQE of 2.67 x 10^5% has been achieved for GeSe photodetector. The GeS photodetector exhibited a maximum detectivity of 1.74 x 10^{13} Jones.

2. Experimental Details

Materials

Germanium(IV) iodide (GeI_4, 99.999%), selenium dioxide (SeO_2, 99.9%), 1-dodecanethiol (1-DDT, 98%), oleylamine (OAm, 70%), 1-octadecene (ODE, 90%), hexadecylamine (HAD, 90%) were purchased from Sigma-Aldrich. Oleylamine and 1-octadecene were dried under vacuum at 120 °C for 6 h and stored in argon filled glove-box. Toluene (HPLC grade) and ethyl alcohol (HPLC grade) were purchased from Samchun chemicals Korea. All the syntheses were carried out under N_2 using standard Schlenk techniques, and purification procedures were performed in air.

Synthesis of GeS nanosheets: 2 mL of 1-DDT, 3 mL of dried ODE and 2 mL of dried OAm were added to a 25 mL 3-neck round bottom flask inside N_2 filled glove-box. The flask was fitted to a reflux condenser and 0.2 mmol of GeI_4 was added to the mixture with N_2 flow. The mixture was then alternated between vacuum and N_2 to remove water and other impurities. Then the flask was heated to 320 °C under N_2 and allowed to react for 10 h, resulted in a dark purple mixture. The nanosheets were precipitated by adding acetone and centrifuged at 4000 rpm for 3 min. The obtained product was then washed three times with toluene:ethanol mixture (1:1 ratio).

Synthesis of GeSe nanosheets: GeI_4 (0.2 mmol) and SeO_2 (0.225 mmol) were loaded into 25 mL 3-neck round bottom flask along with 3 mL of dried ODE and 3g of HAD. The mixture was dried at 60 °C for 15 min under vacuum. Then the flask was heated to 300 °C under N_2. After 3 h the reaction was cooled down to room temperature and the nanosheets were precipitated using ethanol and centrifuged at 4000 rpm for 3 min. The obtained product was then washed three times with toluene:ethanol mixture (1:1 ratio).

Characterization

X-Ray Diffraction (XRD) measurements were performed on a Rigaku MiniFlex 600 diffractometer, equipped with a Cu Kα X-ray source (λ=1.5418 Å). The nanosheets dispersed in toluene were drop casted onto a microscopic glass substrate to form the films.

Transmission electron microscopy (TEM) images, High-resolution TEM (HRTEM) images, selected area electron diffraction (SAED) patterns were recorded on a Hitachi HF-3300 microscope operating at 300 kV. Samples were prepared by dropping diluted nanosheets solution onto carbon coated copper grids.

Scanning electron microscopy (SEM) images and energy dispersive X-ray spectroscopy (EDS) spectra and EDS elemental mapping images were obtained using a Hitachi SU 8020 scanning electron microscope.

Diffuse reflectance spectra were collected using a Cary 5000 UV-Vis-NIR spectrophotometer measured by recording total reflectance using a DRA 2500 diffuse reflectance accessory (integrating sphere).

Atomic force microscopy (AFM) images were recorded in a non-contact mode using a model PSIA Xe-150 (Park System).

For device fabrication, the GeS and GeSe nanosheets were transferred to a Si/SiO_2 substrate by drop casting much diluted dispersions of nanosheets in toluene. Individual GeS and GeSe photodetector was fabricated using e-beam lithography, followed by deposition of electrodes (Ti (5 nm) and Au (45 nm)) and lift off were performed to pattern electrodes on the individual nanosheets. The photoresponse were recorded using a Keithley 2636A Source Meter under 405 nm laser diode with variation of the light intensity from 7.98 $\mu w/cm^2$ to 1.98 mw/cm^2. The scan voltage was tuned from -3V to 3 V.

DFT calculation

DFT calculations for geometry relaxation and electronic structure were performed by using (Vienna Ab-initio Simulation Package) VASP.[36,37] Projector augmented wave (PAW) pseudopotentials as implemented in VASP were used for describing the interactions between ions and electrons, and the exchange-correlation energy of electrons was described by using the generalised gradient approximation (GGA) with hybrid functional (HSE06) methods.[38-40] The energy cutoff for the plane-wave basis is 260 eV. All atoms were fully relaxed until Hellmann-Feynman force was less than 0.01 eV/Å To integrate the Brillouin zone, 9×5×11 gamma-point mesh was used for the GeS and GeSe.

3. Results and discussion

GeS and GeSe nanosheets were synthesized using one-pot heating up method by heating GeI_4, 1-octadecene, oleylamine, dodecanethiol or selenium dioxide at 300 °C. The purity and crystal structure of the as-synthesized nanosheets were characterized by X-ray diffraction (XRD). Fig. 1a shows the atomic structural model of the GeX (X=S, Se) double layers. GeX (X=S, Se) nanosheets are composed of vertically stacked layer structure by week van der Waals force. Fig. 1b and c show the XRD patterns of as-synthesized GeS and GeSe nanosheets, which match well with the orthorhombic crystal structure (GeS, JCPDS No. 71-0306; GeSe, JCPDS No. 48-1226). No secondary phases or any other impurity phases were detected. The observed strong (400) diffraction peaks for both GeS and GeSe nanosheets show that the nanosheets are oriented along [100].

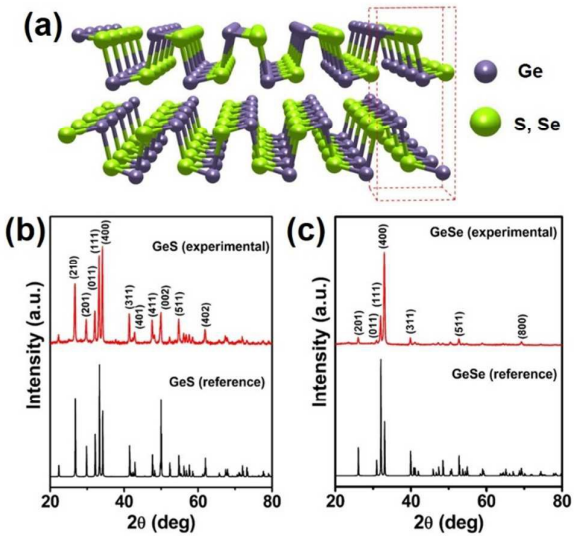

Fig. 1 (a) Crystal structure of orthorhombic GeS and GeSe. XRD patterns of as-synthesized (b) GeS and (c) GeSe nanosheets.

The morphology of the GeS and GeSe nanostructures was studied using scanning electron microscopy (SEM) and transmission electron microscopy (TEM). Large area SEM images in Fig. S1, clearly indicates that most of the products are in 2D nanosheet morphology. As shown in Fig. 2, both the GeS and GeSe have sheet like morphology with lateral dimensions of 5 x 2 μm and 3 x 1 μm for GeS and GeSe, respectively. GeS nanosheet exhibited clear elongated hexagonal morphology (Fig. 2a and b), whereas GeSe nanosheet appeared to consist of smaller hexagonal nanosheets that are stacked together in sheet like morphology (Fig. 2d and e). The corresponding selected area electron diffraction (SAED) patterns are shown in the insets of Fig. 2b and e. The spot patterns clearly indicate the single crystalline nature of the nanosheets. The high resolution TEM (HRTEM) images reveal the lattice spacing of 0.28 and 0.29 nm for GeS and GeSe, respectively (Fig. 2c and f). This is consistent with the {011} set of planes of the orthorhombic crystal structure. The composition of both the nanostructures was analyzed using energy-dispersive X-ray spectroscopy (EDS). EDS measurement show the Ge:S ratio of 1:0.95 in GeS and Ge:Se ratio

of 1:0.9 in GeSe nanosheets (Fig. S2a and S3a in the Supporting Information). In addition, the elemental distribution of the as-synthesized nanosheets was obtained by EDS elemental mapping. Fig. S2b and S3b show that all the elements are distributed homogenously in the nanosheets.

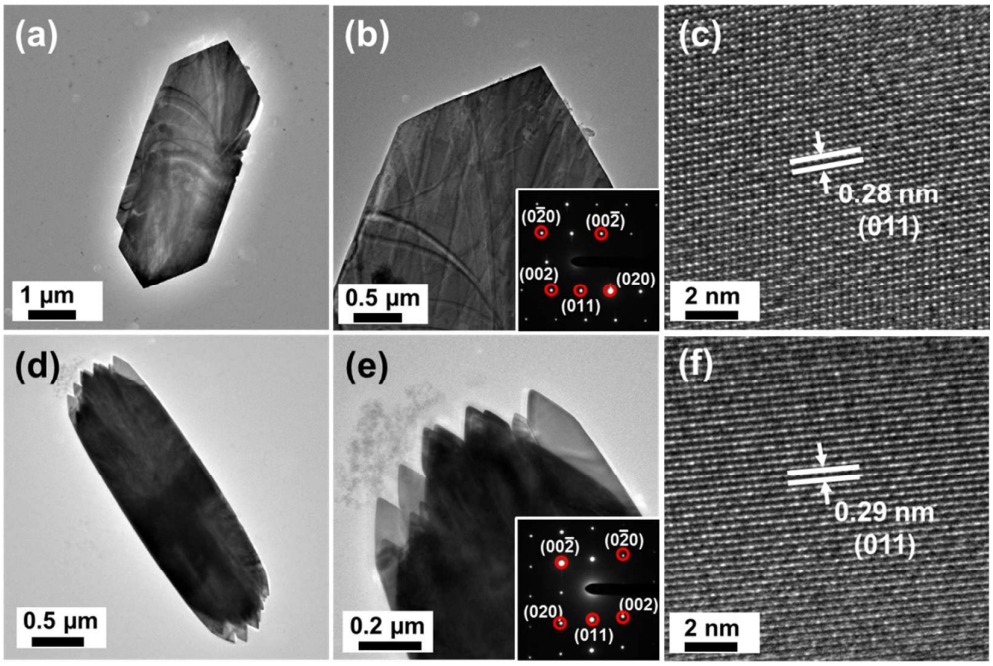

Fig. 2 TEM images of single (a, b) GeS and (d, e) GeSe nanosheet. Insets in 2b and 2e show the corresponding SAED patterns obtained from [100] zone axis. HRTEM images of (c) GeS and (f) GeSe nanosheets.

In order to understand the optical properties of the synthesized nanosheets, we first calculated the electronic band structures of GeS and GeSe using DFT calculation and the results are presented in Fig. 3a and c. The valence band maximum (VBM) and conduction band minimum (CBM) of GeS and GeSe located at the Γ point, resulting in a direct bandgap. The calculated direct bandgap of GeS and GeSe were 1.67 and 1.37 eV, respectively. Diffuse reflectance spectra were used to experimentally determine optical bandgap of the synthesized nanosheets.

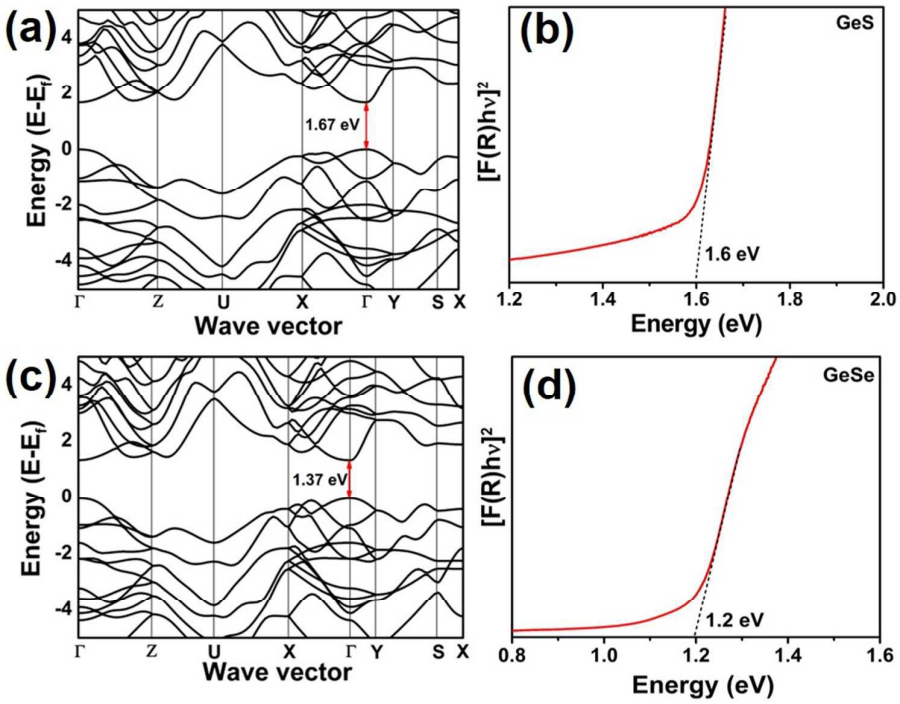

Fig. 3 Band structures of (a) GeS and (c) GeSe. Experimentally calculated direct bandgap of (b) GeS and (d) GeSe nanosheets.

As shown in Fig. S4, the absorption onset for the GeS nanosheets started around 750 nm, whereas for GeSe the absorption onset began around 1150 nm. Kubelka–Munk transformations were performed to determine the optical band gap values. The direct bandgap values were obtained by plotting $[F(R)hv]^2$ *versus* energy. The direct bandgaps of GeS and GeSe were determined to be 1.6 and 1.2 eV, respectively. These values are almost consistent with the theoretically calculated values and previous reports of GeS and GeSe nanostructures.[30,31]

To explore the photoconductive properties of the synthesized GeS and GeSe nanosheets, we fabricated individual GeS and GeSe photodetectors on Si/SiO_2 substrate as shown in the inset at top-left of Fig. 4a. SEM images in the inset of Fig. 4a and c show the devices used to estimate the effective active area of the devices. AFM measurements were used to calculate the thickness of the nanosheets in the devices. 2D AFM mapping results in Fig. S5 yielded a

thickness of 160 nm for GeS and 250 nm for GeSe nanosheets. Fig. 4a and c show the typical I-V curves of individual GeS and GeSe photodetector under dark and illumination under 405 nm laser diode with different incident power. The I–V curves of both GeS and GeSe exhibit nonlinearity, which is attributed to the Schottky barrier contact arising from the mismatch of the work functions between the Ti/Au electrodes and GeS or GeSe nanosheets.[31,41]

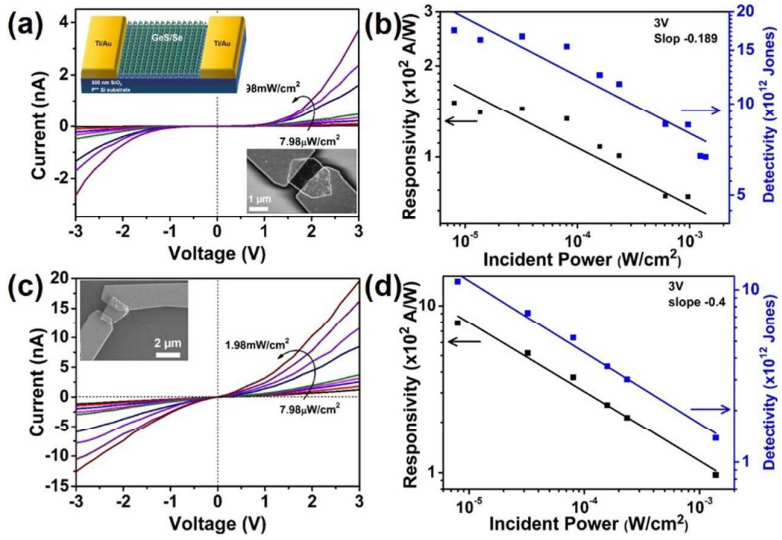

Fig. 4 *I-V* output curves of the (a) GeS and (c) GeSe photodetectors under dark and illumination at 405 nm with different incident intensities. Calculated responsivity and detectivity of the (b) GeS and (d) GeSe devices at applied bias of 3 V. Insets in 4a show the device schematic and SEM image of GeS device. Inset in 4c shows the SEM image of GeSe device.

As shown in Fig. 4a and c, both the GeS and GeSe devices exhibited high photoresponse characteristics. The photocurrent significantly increased under light illumination compared to that of the dark current due to the photogenerated electron-hole pair which increased the conductivity. Upon 405 nm light excitation with the intensity of 1.98 mW/cm^2, the photocurrent reached a maximum value of 3.7 and 20 nA for GeS and GeSe, respectively. In addition, the photocurrent of both the devices exhibited strong dependence to the incident

light intensity. The photocurrents increased with increasing light intensity. This is consistent with the fact that the charge carrier photogeneration efficiency is proportional to the absorbed photon flux.

Photoresponsivity (R) and external quantum efficiency (EQE) are the two critical parameters used to evaluate the performance of photodetectors. Photoresponsivity is defined as the photocurrent generated per unit power of the incident light on the effective area and EQE is the number of electrons detected per incident photon of a photoconductor. R and EQE can be calculated by

$$R = \Delta I / PA \quad (1)$$

and,

$$EQE = hcR / e\lambda \quad (2)$$

where ΔI is the photocurrent ($I_{photocurrent}$-$I_{dark\ current}$); P is the light power intensity irradiated on the nanosheet; A is the effective area of photodetector; h is Planck's constant; c is the speed of light; e is electron charge; and λ is the excitation wavelength. Based on the above equations, the R is calculated to be 173 and 870 AW^{-1} for GeS and GeSe, respectively under illumination of 405 nm with intensity of 1.98 mW cm^{-2} at a bias of 3 V. The calculated EQE of GeS and GeSe is 5.32 x 10^4 and 2.67 x 10^5 %, respectively. These values are several orders of magnitude higher than that of previous reported for graphene and many other metal chalcogenide nanosheet photodetectors. The photodetector characteristics of various 2D nanosheets are listed in table 1.

Table 1. Comparison of the parameters of our GeS and GeSe devices to the reported 2D material based photodetectors.

Photodetectors	Synthesis Condition	Excitation Wavelength (nm)	Responsivity (AW^{-1})	(EQE) (%)	Response Time (s)	Ref
GaS	Mechanical exfoliation	254	4.2	2.05×10^3	0.03	16
GeS	Vapor deposition	530	139.9	32.7×10^3	0.85	29
GeSe	Vapor deposition and mechanical exfoliation	808	3.5	5.37×10^2	0.1	31
GaTe	Vapor deposition	473	0.03	8	0.054	41
SnS_2	Vapor deposition	473	100	33×10^3	0.022	42
GeS	Solution synthesis	405	173	5.32×10^4	0.11	This work
GeSe	Solution synthesis	405	870	2.67×10^5	0.15	This work

Besides photoresponsivity and EQE, the specific detectivity (D*) is also one of the key figure-of-merits for a photodetector, which is expressed as

$$D^* = RA^{1/2}/(2eI_d)^{1/2} \qquad (3)$$

where R is the responsivity, A is the effective area of the detector, *e* is the absolute value of electron charge, and I_d is the dark current density. Fig. 4b and d shows the calculated D* of the GeS and GeSe photodetector at different light intensities. The calculated detectivity for GeS and GeSe is 1.74×10^{13} and 1.12×10^{13} Jones, respectively.

Fig. 5 shows photocurrent-time (I_{ph}-t) response measured in the dark and under illumination using a laser diode at 405nm as a function of light intensity at fixed applied bias of 2V. Fig. 5a and c shows the response time of photocurrent related to ON-OFF switching with various incident light powers from 1.38 mW/cm^2 to 1.98 mW/cm^2 under 405 nm laser at V_{DS} = 2V. The rise in photocurrent upon turning on the incident light, followed by decay to dark current without any tail after removing the incident light. Both the devices exhibited good stability and reproducibility.

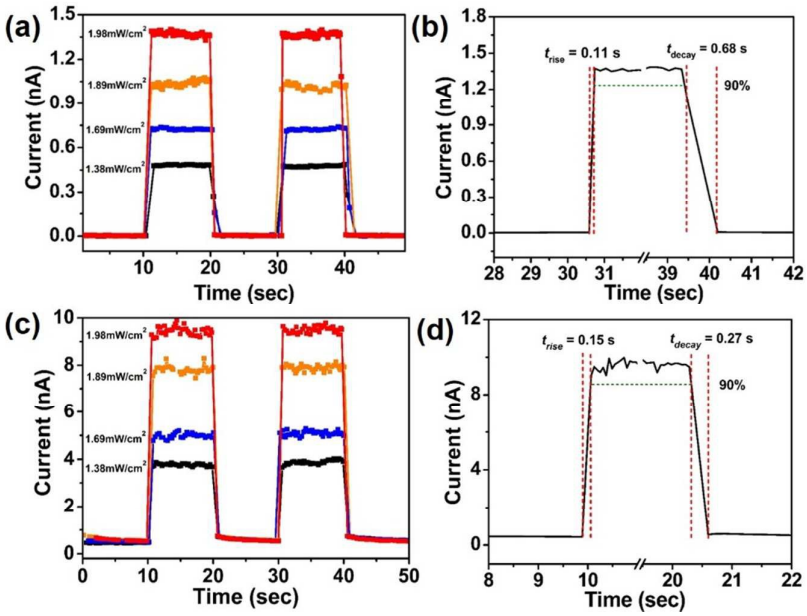

Fig. 5 Time-dependent photocurrent response of (a) GeS and (c) GeSe devices to laser light illuminations with different light intensities at fixed bias of 2 V. The magnified parts of one response cycle showing the rise and fall time of the (b) GeS and (d) GeSe nanosheet devices.

The photocurrent is further increased by increasing the intensity of light while response time is not changed significantly. As shown in Fig. 5c and d, we calculated the rise and decay time of the devices using a single exponential function. For GeS the rise time and the decay time were calculated be 0.11 and 0.68 s, respectively. For GeSe device the rise and fall time were around 0.15 and 0.27 s respectively. In literature, both the GeS and GeSe have been reported to have a long fall time (~ 4 s) due to presence of charge carrier traps and defect states.[27,29] The fast decay time in our devices can be attributed by high quality of the solution synthesized nanosheets.

4. Conclusions

In summary, we have reported facile one-pot solution based synthesis methods for GeS and GeSe nanostructures. Both the GeS and GeSe have sheet like morphology with lateral dimensions in micrometers. GeS and GeSe nanosheets were found to have a direct bandgap value of 1.6 and 1.2 eV, respectively. Photodetectors made from these nanosheets exhibited very sensitive, stable and fast photoresponse at 405 nm excitation. The GeS photodetector exhibited a maximum detectivity of 1.74×10^{13} Jones, and GeSe photodetector exhibited high responsivity of 870 AW^{-1} and high EQE of 2.67×10^{5} %. These results are very promising and suggest that both the GeS and GeSe nanosheets are potential narrow bandgap semiconductors for high performance photodetectors. However, the thickness of the synthesized nanosheets are relatively high, further improvements in device performance can be possible by decreasing the thickness of the nanosheets.

Acknowledgements

This work was supported by the DGIST R&D Program of the Ministry of Science, ICT and Future Planning (15-BD-0401) and the Leading Foreign Research Institute Recruitment Program (Grant No. 2012K1A4A3053565) through NRF funded by MEST. We thank H. S. Jang, S. K. Jeon (CCRF DGIST) for discussions of Electron beam- and Photo-lithography system. Nano-device fabrication was carried out in CCRF of DGIST.

References

1. Q. H. Wang, K. Kalantar-Zadeh, A. Kis, J. N. Coleman and M. S. Strano, *Nat. Nanotech*., 2012, **7**, 699.
2. G. Eda and S. A. Maier, *ACS Nano*, 2013, **7**, 5660.
3. F. Bonaccorso, L. Colombo, G. Yu, M. Stoller, V. Tozzini, A. C. Ferrari, R. S. Ruoff and V. Pellegrini, *Science*, 2015, **347,** 1246501.
4. J. H. Han, S. Lee and J. Cheon, *Chem. Soc. Rev*., 2013, **42**, 2581.
5. C. Tan and H. Zhang, *Chem. Soc. Rev*., 2015, **44**, 2713.
6. Y. D. Kim, H. Kim, Y. Cho, J. H. Ryoo, C.-H. Park, P. Kim, Y. S. Kim, S. Lee, Y. Li, S.-N. Park, Y. Shim Yoo, D. Yoon, V. E. Dorgan, E. Pop, T. F. Heinz, J. Hone, S.-H. Chun, H. Cheong, S. W. Lee, M.-H. Bae and Y. D. Park, *Nat Nanotech*., 2015, **10**, 676.
7. Q. Bao and K. P. Loh, *ACS Nano*, 2012, **6**, 3677.
8. W. Yuan and G. Shi, *J. Mater. Chem. A*, 2013, **1**, 10078.
9. S. Z. Butler, S. M. Hollen, L. Cao, Y. Cui, J. A. Gupta, H. R. Gutiérrez, T. F. Heinz, S. S. Hong, J. Huang, A. F. Ismach, E. Johnston-Halperin, M. Kuno, V. V. Plashnitsa, R. D. Robinson, R. S. Ruoff, S. Salahuddin, J. Shan, L. Shi, M. G. Spencer, M. Terrones, W. Windl and J. E. Goldberger, *ACS Nano*, 2013, **7**, 2898.
10. M. Chhowalla, H. S. Shin, G. Eda, L.-J. Li, K. P. Loh and H. Zhang, *Nat. Chem*., 2013, **5**, 263.
11. K. J. Koski and Y. Cui, *ACS Nano*, 2013, **7**, 3739.
12. L. Li, Z. Chen, Y. Hu, X. Wang, T. Zhang, W. Chen and Q. Wang, *J. Am. Chem. Soc*., 2013, **135**, 1213.
13. Z. Fang, S. Hao, L. Long, H. Fang, T. Qiang and Y. Song, *CrystEngComm*, 2014, **16**, 2404.
14. O. Lopez-Sanchez, D. Lembke, M. Kayci, A. Radenovic and A. Kis, *Nat. Nanotech*., 2013, **8**, 497.
15. J. Xia, X. Huang, L.-Z. Liu, M. Wang, L. Wang, B. Huang, D.-D. Zhu, J.-J. Li, C.-Z. Gu and X.-M. Meng, *Nanoscale*, 2014, **6**, 8949.
16. P. Hu, L. Wang, M. Yoon, J. Zhang, W. Feng, X. Wang, Z. Wen, J. C. Idrobo, Y. Miyamoto, D. B. Geohegan and K. Xiao, *Nano Lett*., 2013, **13**, 1649.
17. S. Yang, Y. Li, X. Wang, N. Huo, J.-B. Xia, S.-S. Li and J. Li, *Nanoscale*, 2014, **6**, 2582.
18. P. Hu, Z. Wen, L. Wang, P. Tan and K. Xiao, *ACS Nano*, 2012, **6**, 5988.
19. R. B. Jacobs-Gedrim, M. Shanmugam, N. Jain, C. A. Durcan, M. T. Murphy, T. M. Murray, R. J. Matyi, R. L. Moore and B. Yu, *ACS Nano*, 2014, **8**, 514.
20. W. Feng, J.-B. Wu, X. Li, W. Zheng, X. Zhou, K. Xiao, W. Cao, B. Yang, J.-C. Idrobo, L. Basile, W. Tian, P. Tan and P. Hu, *J. Mater. Chem. C*, 2015, **3**, 7022.
21. P. D. Antunez, J. J. Buckley and R. L. Brutchey, *Nanoscale*, 2011, **3**, 2399.
22. G. Xiao, Y. Wang, J. Ning, Y. Wei, B. Liu, W. W. Yu, G. Zou and B. Zou, *RSC Adv*., 2013, **3**, 8104.
23. L. Makinistian and E. A. Albanesi, *Phy. Rev. B*, 2006, **74**, 045206.
24. L. Makinistian and E. A. Albanesi, *J. Phys.:Condens. Matter.* **2007**, *19*, 186211.
25. Y. J. Cho, H. S. Im, Y. Myung, C. H. Kim, H. S. Kim, S. H. Back, Y. R. Lim, C. S. Jung, D. M. Jang, J. Park, E. H. Cha, S. H. Choo, M. S. Song and W. I. Cho, *Chem. Commun*., 2013, **49**, 4661.
26. Y. J. Cho, H. S. Im, H. S. Kim, Y. Myung, S. H. Back, Y. R. Lim, C. S. Jung, D. M. Jang, J. Park, E. H. Cha, W. I. Cho, F. Shojaei and H. S. Kang, *ACS Nano*, 2013, **7**, 9075.
27. H. S. Im, Y. R. Lim, Y. J. Cho, J. Park, E. H. Cha and H. S. Kang, *J. Phys. Chem. C*, 2014, **118**, 21884.
28. C. Li, L. Huang, G. P. Snigdha, Y. Yu and L. Cao, *ACS Nano*, 2012, **6**, 8868.

29. C. Lan, C. Li, Y. Yin, H. Guo and S. Wang, *J. Mater. Chem. C*, 2015, **3**, 8074.
30. S. M. Yoon, H. J. Song and H. C. Choi, *Adv. Mater*., 2010, **22**, 2164.
31. B. Mukherjee, Y. Cai, H. R. Tan, Y. P. Feng, E. S. Tok and C. H. Sow, *ACS Appl. Mater. Interfaces*, 2013, **5**, 9594.
32. D. D. Vaughn Ii, R. J. Patel, M. A. Hickner and R. E. Schaak, *J. Am. Chem. Soc*., 2010, **132**, 15170.
33. D. Vaughn, D. Sun, S. M. Levin, A. J. Biacchi, T. S. Mayer and R. E. Schaak, *Chem. Mater*., 2012, **24**, 3643.
34. D.-J. Xue, J. Tan, J.-S. Hu, W. Hu, Y.-G. Guo and L.-J. Wan, *Adv. Mater*., 2012, **24**, 4528.
35. L. Shi, Y. Li and Y. Dai, *ChemPlusChem*, 2015, **80**, 630.
36. G. Kresse and J. Furthmuller, *Phys. Rev. B*, 1996, **54**, 11169.
37. G. Kresse and D. Joubert, *Phys. Rev. B*, 1999, **59**, 1758.
38. P. E. Blochl, *Phys. Rev. B*, 1994, **50**, 17953.
39. J. Heyd, G. E. Scuseria and M. Ernzerhof, *J. Chem. Phys*., 2003, **118**, 8207.
40. J. Heyd, G. E. Scuseria and M. Ernzerhof, *J. Chem. Phys*., 2006, **124**, 219906.
41. Z. Wang, M. Safdar, M. Mirza, K. Xu, Q. Wang, Y. Huang, F. Wang, X. Zhan and J. He, *Nanoscale*, 2015, **7**, 7252.
42. Y. Huang, H.-X. Deng, K. Xu, Z.-X. Wang, Q.-S. Wang, F.-M. Wang, F. Wang, X.-Y. Zhan, S.-S. Li, J.-W. Luo and J. He, *Nanoscale*, 2015, **7**, 14093.

Graphical Abstract